



Effect of distributed axial loading on dynamic stability and buckling analysis of a viscoelastic DWCNT conveying viscous fluid flow

Kianoosh Mohammadi¹ · Mohammad Mostafa Barouti¹ · Hamed Safarpour¹ · Majid Ghadiri¹

Received: 23 May 2018 / Accepted: 18 January 2019 / Published online: 25 January 2019
© The Brazilian Society of Mechanical Sciences and Engineering 2019

Abstract

In this article, dynamic stability and buckling analysis of a double-walled carbon nanotube (DWCNT) under distributed axial force are investigated. The visco-Pasternak model is used to simulate the elastic medium between nanotubes considering the effects of spring, shear and damping of the elastic medium. This system is conveying viscous fluid, and the relevant force is calculated by modified Navier–Stokes relation considering slip boundary condition and Knudsen number. The nanostructure is modeled as two orthotropic moderately thick cylindrical shells, and the effects of small-scale and structural damping are accounted based on modified couple stress and Kelvin–Voigt theories. The governing equations and boundary conditions are developed using Hamilton’s principle and solved with the aid of Navier and generalized differential quadrature methods. In this research, the dynamic instability occurs in the viscoelastic DWCNT conveying viscous fluid flow as the natural frequency becomes equal to zero. The results show that the velocity of viscous fluid flow, axial load, mode number, length-to-radius ratio, radius-to-thickness ratio, visco-Pasternak foundation and the boundary conditions play important roles on the critical pressure and natural frequency of the viscoelastic DWCNT conveying viscous fluid flow under axial force.

Keywords Kelvin–Voigt theory · DWCNT · Buckling analysis · Dynamic stability · Modified Navier–Stokes relation · GDQM

1 Introduction

The mechanical behaviors of conveying fluid carbon nanotubes need to be investigated in the presence of different external effects due to the wide range of their applications in various engineering components such as nanocontainers for gas storage [1] and drug delivery devices [2]. These kinds of researches conduct engineers to more accurate designs, and in recent years scholars have studied various aspects of this field. Here some of them are reviewed. Tang and Yang [3] conducted a study on post-buckling and nonlinear vibration of functionally graded pipes with internal fluid flow. They analyzed the influences of flow velocity, fluid density and the initial stress on the responses. In some experimental

researches [4–6] which is the most reliable method, it was shown that in submicron scales, mechanical properties are size dependent, and consequently, classical theories cannot be used. Molecular dynamic simulation is a useful numerical method to predict nanostructures behavior, but it is often time-consuming. Therefore, non-classical theories are employed to consider the size effects and they can be calibrated by molecular dynamic simulation [7–9] to achieve more accurate responses. In addition, this material can be used in electrical devices such as those mentioned in Refs [10–12]. Nonlocal elasticity theory expresses the stress field at a reference point that is assumed to be dependent on the strains at all points in the body, not only at the reference point [13]. Many vibrational studies [14–18] have paid attention to nonlocal effects using nonlocal elasticity theory. Lee et al. [19] employed nonlocal elasticity theory to analyze the effects of flow velocity on the vibration frequency and mode shapes of the single-walled carbon nanotube conveying fluid flow. Their results showed that increasing the nonlocal parameter reduces the real component of frequency, and this behavior is more obvious in lower flow velocities and higher modes. Arani et al. [20, 21] developed cylindrical

Technical Editor: Wallace Moreira Bessa, D.Sc.

✉ Majid Ghadiri
ghadiri@eng.ikiu.ac.ir

¹ Department of Mechanics, Faculty of Engineering, Imam Khomeini International University, 3414916818, Qazvin, Iran

shell model to investigate the nonlinear and nonlocal vibration of embedded double-walled carbon and boron nitride nanotubes conveying fluid. They demonstrated that the critical flow velocity of proposed models is inversely related to the nonlocal parameter, so that an increase in the parameter reduces the critical flow velocity. Bahaadini and hosseini [22] worked on the free vibration and flutter instability of viscoelastic cantilever carbon nanotubes conveying fluid flow using nonlocal elasticity theory and slip boundary condition. Tang and Yang [23] employed the Euler–Bernoulli beam and Eringen’s theory to develop a model of conveying fluid nanotubes made of functionally graded materials along the both axial and radial directions. They proved this kind of materials distribution can dramatically change the natural frequency and structural stability of system. Wang et al. [24] studied the variations of natural frequency for cantilevered CNTs conveying fluid in the presence of magnetic field. They showed an increase in magnetic field makes the system stiffer so that critical flow velocity increases; moreover, in case the magnetic field parameter is greater than flow velocity, the CNT system becomes stable. Askari and Esmailzadeh [25] proposed a nonlocal Euler–Bernoulli beam model to examine vibration primary resonance and linear natural frequency of a CNT conveying fluid flow. Zhang et al. [26] studied the nonlocal and surface effects on longitudinal wave propagation of a piezoelectric nanoplate. Based on their result, increasing the wave number and scale coefficient can enhance the dispersion degree. Zhang et al. [27] considered the quantum effect in the study of fluid induced vibration of a nonlocal Euler–Bernoulli beam as a single-walled carbon nanotube. They showed that the root of mean-squared amplitude of the vibration estimated by quantum theory is lower than those of the law of energy equipartition. Some studies paid attention to pulsating fluid flow. Azrar et al. [28] analyzed the effects of fluid pulsation, nonlocal parameter and viscoelastic carbon nanotube parameters on dynamics instability of a SWCNT with internal fluid flow. Mirfazal et al. [29] modeled a double-walled carbon nanotube using higher-order sinusoidal shear order deformation shell theory and investigated the influence of pulsating flow on the dynamic behavior of system.

Although nonlocal elasticity theory is a size-dependent continuum mechanics theory which is appropriate to predict the vibrational behavior of nanostructures, the strain gradient theory and modified couple stress theory seem to have a better agreement with experimental reports [30]. Researches have widely paid attention to the effects of various parameters on the buckling and vibration characteristics of submicron shells based on the strain gradient theory [31–35] and the modified couple stress theory [36–40]. Here it is worth referencing some recent studies on static and dynamic analysis of carbon nanotubes conveying fluid flow in the framework of these theories. Zeighampour and

Beni [41] conducted a study on the vibration analysis of double-walled carbon nanotubes conveying fluid using the modified couple stress theory (MCST) and Donnell’s shell model. Ansari et al. [42] studied the vibration behavior and instability of cylindrical microshells made of functionally graded (FG) materials and containing flowing fluid. They showed that increasing the value of material property gradient index of FGM microshell enhances the natural frequency and the critical flow velocity. Tang et al. [43] developed a nonlinear model for three-dimensional vibration of curved microtubes conveying fluid with clamped–clamped boundary conditions based on the modified couple stress theory. They considered the in-plane and out-of-plane bending motions, the axial motion and the twist angle of microtube in their model. Safarpour and Ghadiri [44] studied the critical velocity of viscous fluid flow and the free vibration analysis of a spinning single-walled carbon nanotube. Hu et al. [45] presented a nonlinear theoretical model to explore the possible size-dependent nonlinear responses based on the modified couple stress theory for cantilevered micropipes conveying fluid. Guo et al. [46] studied three-dimensional nonlinear vibration of cantilever micropipes conveying fluid. They proved increasing the material length scale enlarges the region of mass ratio for stable planar periodic motion. Yang et al. [47] analyzed nonlinear free vibration of a microtube conveying microfluid via modified couple stress theory. In this work, geometric nonlinearity due to midplane stretching was accounted.

According to Mindlin’s strain gradient theory, Sotudeh and Afrahim [48] studied the small-scale nonlinear vibration of micropipes conveying fluid. They proved material length scale and FG power index have significant influences on the fundamental natural frequency and fluid critical velocity. Ghorbanpour et al. [49] conducted a study on dynamic instability of a double-walled carbon nanotube with internal pulsating fluid flow based on sinusoidal shear deformation beam theory. They employed strain gradient and Gurtin–Morduch elasticity theories to capture the effects of size and surface, respectively. Ansari et al. [50] worked on the thermo mechanical vibration and instability of the functionally graded nanoshells in the presence of inner fluid flow. They [51] also considered the surface effect in the nonlinear vibration of conveying fluid nanoscale pipes. Ghazavi et al. [52] applied the second gradient theory on Euler–Bernoulli beam model to study nonlinear vibration of conveying fluid nanotubes for the first time. They indicated that considering the hardening effects, nonlinear instabilities are obtained more precisely. Li et al. [53] derived Timoshenko and Euler–Bernoulli beam models for microtubes conveying fluid flow using the nonlocal strain gradient theory (NSGT) in which both nonlocal and material length-scale effects are considered. Mohammadi et al. [54] developed FSDT cylindrical shell model based on NSGT for analyzing

vibration behavior of CNTs. Mahinzare et al. [55] investigated the effects of size-dependent parameters of NSGT on critical flow velocity in CNTs with internal water flow. They indicated nonlocal parameter shrinks the stability region, whereas material length scale extends this region. In addition, current nanostructure can be used in smart systems [56, 57]. There are some cases in engineering designs that expose cylindrical shells to axial forces, so some researchers have paid attention to this condition. In an analytical study, Sheng and Wang [58] investigated the nonlinear vibration of cylindrical shell under the axial loads in a thermal environment. Jansen and Rolfes [59] studied the nonlinear vibration of laminated cylindrical shells subjected to static axial loads under different boundary conditions. Sofiyev [60] employed the shear deformation theory to analyze the vibration and stability of a conical FG shell subjected to compressive axial force. Liang and Su [61] developed a frequency–amplitude plane to obtain the stability regions for a single-walled carbon nanotube conveying pulsating fluid flow under tensile force. In this study, it was shown that axial tensile force significantly changes the natural frequency.

According to the above literature, some scientific papers studied the effects of fluid flow or axial external force on the dynamic instability of microbeams, microshells and other micronanostructures, separately. But there is no research on the vibration analysis of CNTs considering the effects of both viscous fluid flow and distributed axial load in one cylindrical nanoshell model; therefore, in this paper for the first time, an investigation is made on the dynamic stability analysis of a viscoelastic double-walled carbon nanotube conveying viscous fluid flow and subjected to distributed axial force in the framework of FSDT and modified couple stress theory. Using the Hamilton's principle and GDQ solution method, critical values of axial force and flow velocity are determined; moreover, the effects of some factors such as the effect of flow velocity, axial load, mode number, length-to-radius ratio, radius-to-thickness ratio, visco-Pasternak foundation and boundary conditions are investigated on the critical pressure and natural frequency of the viscoelastic

DWCNT with inner viscous fluid flow subjected to axial force.

2 Formulation

2.1 Governing equations of motion and corresponding boundary conditions

Figure 1 presents a schematic of DWCNT conveying viscous fluid subjected to the mechanical loading. Moreover, this figure demonstrates the effect of the visco-Pasternak foundation between the two walls and the surroundings of this structure. L , R and h denote the length, radius and the thickness of the DWCNT, respectively. In this study, the DWCNT is modeled as two cylindrical viscoelastic shells. According to the FSDT, the displacement field of each cylindrical shell along the three directions of x , θ , z is as follows:

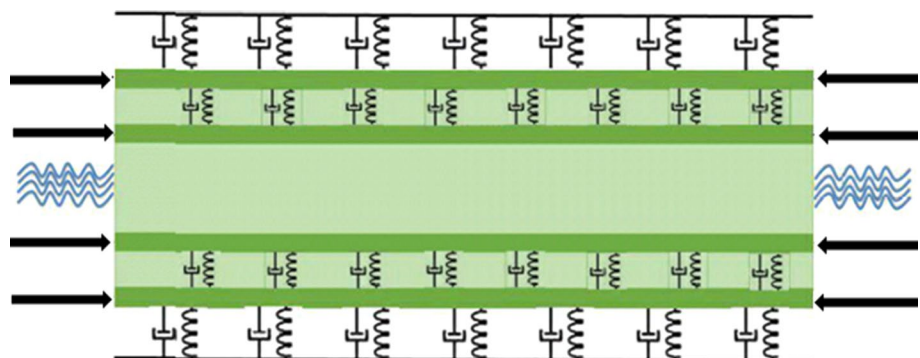
$$\begin{aligned} U(x, \theta, z, t) &= u(x, \theta, t) + z\psi_x(x, \theta, t) \\ V(x, \theta, z, t) &= v(x, \theta, t) + z\psi_\theta(x, \theta, t) \\ W(x, \theta, z, t) &= w(x, \theta, t) \end{aligned} \quad (1)$$

where $u(x, \theta, t)$, $v(x, \theta, t)$ and $w(x, \theta, t)$ represent the displacements in axial, circumferential and radial directions, respectively. $\psi_\theta(x, \theta, t)$ and $\psi_x(x, \theta, t)$ are the rotations about the circumferential and axial directions. In addition, strain tensor is expressed as:

$$\begin{aligned} \varepsilon_{ij} &= \frac{1}{2}(A_{i,j} + A_{j,i}), \\ \chi_{ij}^s &= \frac{1}{2}(\varphi_{i,j} + \varphi_{j,i}), \\ m_{ij}^s &= 2l^2 \mu(\hat{z}) \chi_{ij}^s. \end{aligned} \quad (2)$$

In Eq. (2) u_i and θ_i represent the components of displacement vector and infinitesimal rotation vector, respectively. Furthermore, l is the parameter which denotes the additional and independent material length-scale parameter which

Fig. 1 A viscoelastic DWCNT conveying viscous fluid flow subjected to distributed axial force



relates to the symmetric rotation gradients. The stress–strain equations in plane stress cases are written as follows for the elastic isotropic moderately thick cylindrical shell model:

$$\begin{Bmatrix} \sigma_{xx} \\ \sigma_{\theta\theta} \\ \sigma_{x\theta} \\ \sigma_{\theta z} \\ \sigma_{xz} \end{Bmatrix} = \begin{bmatrix} \frac{E}{1-\nu^2} & \frac{E\nu}{1-\nu^2} & 0 & 0 & 0 \\ \frac{E\nu}{1-\nu^2} & \frac{E}{1-\nu^2} & 0 & 0 & 0 \\ 0 & 0 & \frac{E}{2(1+\nu)} & 0 & 0 \\ 0 & 0 & 0 & \frac{E}{2(1+\nu)} & 0 \\ 0 & 0 & 0 & 0 & \frac{E}{2(1+\nu)} \end{bmatrix} \begin{Bmatrix} \epsilon_{xx} \\ \epsilon_{\theta\theta} \\ 2\epsilon_{x\theta} \\ 2\epsilon_{\theta z} \\ 2\epsilon_{xz} \end{Bmatrix} \quad (3)$$

The principle of minimum potential energy is used in order to derive the equations of motion and the associated boundary conditions:

$$\int_{t_1}^{t_2} (\delta T - \delta U + \delta W) dt = 0 \quad (4)$$

where U and T are strain and kinetic energies, respectively. W is the work done by the external forces acting on the wall. The strain energy of a cylindrical shell includes classical strain energy U_1 and non-classical strain U_2 . Therefore, the variation of strain energy would be written as follows:

$$\delta U = \delta U_1 + \delta U_2 \quad (5)$$

where

$$\delta U_1 = \frac{1}{2} \iiint_V (\sigma_{ij} \delta \epsilon_{ij}) dV = \iint_A \left\{ \begin{aligned} & \left(N_{xx} \frac{\partial}{\partial x} \delta u + M_{xx} \frac{\partial}{\partial x} \delta \psi_x \right) + N_{\theta\theta} \left(\frac{1}{R} \frac{\partial}{\partial \theta} \delta v + \frac{\delta w}{R} \right) \\ & + M_{\theta\theta} \frac{1}{R} \frac{\partial}{\partial \theta} \delta \psi_\theta + Q_{xz} \left(\delta \psi_x + \frac{\partial}{\partial x} \delta w \right) \\ & + N_{x\theta} \left(\frac{1}{R} \frac{\partial}{\partial \theta} \delta u + \frac{\partial}{\partial x} \delta v \right) + M_{x\theta} \left(\frac{1}{R} \frac{\partial}{\partial \theta} \delta \psi_x + \frac{\partial}{\partial x} \delta \psi_\theta \right) \\ & + Q_{z\theta} \left(\delta \psi_\theta + \frac{1}{R} \frac{\partial}{\partial \theta} \delta w - \frac{\delta v}{R} \right) \end{aligned} \right\} R dx d\theta$$

$$\delta U_2 = \frac{1}{2} \iiint_V (m_{ij}^s \delta \chi_{ij}^s) dV = \iint_A \left\{ \begin{aligned} & \left(-\frac{Y_{\theta\theta}}{2R^2} + \frac{Y_{zz}}{2R^2} \right) \frac{\partial}{\partial \theta} \delta u - \left(\frac{Y_{\theta z}}{2R^2} \right) \frac{\partial^2}{\partial \theta^2} \delta u - \left(\frac{Y_{zx}}{2R} \right) \frac{\partial^2}{\partial \theta \partial x} \delta u \\ & + \left(\frac{Y_{\theta\theta}}{2R} - \frac{Y_{xx}}{2R} \right) \frac{\partial}{\partial x} \delta v + \left(\frac{Y_{xz}}{2} \right) \frac{\partial^2}{\partial x^2} \delta v - \left(\frac{Y_{\theta x}}{2R^2} \right) \left(\frac{\partial}{\partial \theta} \right) \delta v \\ & + \left(\frac{Y_{\theta z}}{2R} \right) \frac{\partial^2}{\partial \theta \partial x} \delta v + \left(\frac{Y_{xz}}{2R^2} \right) \delta v + \left(\frac{Y_{\theta z}}{2R} \right) \frac{\partial}{\partial x} \delta w - \left(\frac{Y_{\theta x}}{2} \right) \frac{\partial^2}{\partial x^2} \delta w \\ & - \left(\frac{Y_{zx}}{2R^2} \right) \frac{\partial}{\partial \theta} \delta w + \left(\frac{Y_{x\theta}}{2R^2} \right) \frac{\partial^2}{\partial \theta^2} \delta w + \left(-\frac{Y_{\theta\theta}}{2R} + \frac{Y_{xx}}{2R} \right) \frac{\partial^2}{\partial \theta \partial x} \delta w \\ & + \left(\frac{Y_{x\theta}}{2} \right) \frac{\partial}{\partial x} \delta \psi_x + \left(\frac{Y_{\theta\theta}}{2R} - \frac{Y_{xx}}{2R} \right) \frac{\partial}{\partial \theta} \delta \psi_x - \left(\frac{T_{zx}}{2R} \right) \frac{\partial^2}{\partial \theta \partial x} \delta \psi_x \\ & - \left(\frac{Y_{z\theta}}{2R} \right) \delta \psi_x - \left(\frac{Y_{x\theta}}{2R} \right) \frac{\partial}{\partial \theta} \delta \psi_\theta + \left(\frac{Y_{\theta\theta}}{2R} - \frac{Y_{xx}}{2R} + \frac{Y_{zz}}{2} \right) \frac{\partial}{\partial x} \delta \psi_\theta \\ & + \left(\frac{T_{z\theta}}{2R} \right) \frac{\partial^2}{\partial \theta \partial x} \delta \psi_\theta - \left(\frac{T_{z\theta}}{2R^2} \right) \frac{\partial^2}{\partial \theta^2} \delta \psi_x + \left(\frac{T_{xz}}{2} \right) \frac{\partial^2}{\partial x^2} \delta \psi_\theta - \frac{Y_{xz}}{2R} \delta \psi_\theta \end{aligned} \right\} R dx d\theta \quad (6)$$

where classical and non-classical force and momentum are defined as below:

$$\begin{aligned} (N_{xx}, N_{\theta\theta}, N_{x\theta}) &= \int_{-h/2}^{h/2} (\sigma_{xx}, \sigma_{\theta\theta}, \sigma_{x\theta}) dz, \\ (M_{xx}, M_{\theta\theta}, M_{x\theta}) &= \int_{-h/2}^{h/2} (\sigma_{xx}, \sigma_{\theta\theta}, \sigma_{x\theta}) z dz, \\ (Q_{xz}, Q_{z\theta}) &= \int_{-h/2}^{h/2} k_s (\sigma_{xz}, \sigma_{z\theta}) dz, \\ (Y_{xx}, Y_{\theta\theta}, Y_{zz}, Y_{x\theta}, Y_{xz}, Y_{z\theta}) &= \int_{-h/2}^{h/2} (m_{xx}, m_{\theta\theta}, m_{zz}, m_{x\theta}, m_{xz}, m_{z\theta}) dz, \\ (T_{xx}, T_{\theta\theta}, T_{zz}, T_{x\theta}, T_{xz}, T_{z\theta}) &= \int_{-h/2}^{h/2} (m_{xx}, m_{\theta\theta}, m_{zz}, m_{x\theta}, m_{xz}, m_{z\theta}) z dz \end{aligned} \quad (7)$$

Furthermore, the kinetic energy of a DWCNT can be expressed as:

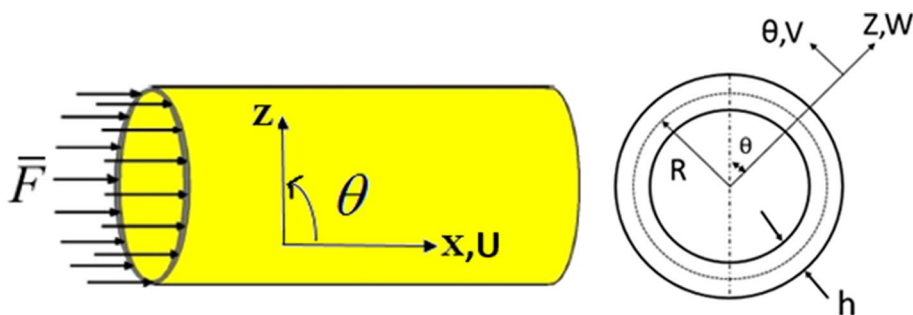
$$\delta T = \int_Z \iint_A \rho \left\{ \begin{aligned} & \left(\frac{\partial u}{\partial t} + z \frac{\partial \psi_x}{\partial t} \right) \left(\frac{\partial}{\partial t} \delta u + z \frac{\partial}{\partial t} \delta \psi_x \right) \\ & + \left(\frac{\partial v}{\partial t} + z \frac{\partial \psi_\theta}{\partial t} \right) \left(\frac{\partial}{\partial t} \delta v + z \frac{\partial}{\partial t} \delta \psi_\theta \right) + \left(\frac{\partial w}{\partial t} \right) \delta w \end{aligned} \right\} R dz dx d\theta \quad (8)$$

The first variation of the corresponding work to the external mechanical loading is [62]:

$$\delta W_1 = \iint_A \left[(\bar{F}) \frac{\partial w}{\partial x} \frac{\partial \delta w}{\partial x} + (\bar{F}) \frac{\partial v}{\partial x} \frac{\partial \delta v}{\partial x} \right] R dx d\theta \quad (9)$$

where $\bar{F} = F/2\pi R$ is the force per length unit of the shell circumference and the axial stress is uniformly distributed along the thickness. Figure 2 shows a schematic of the DWCNT under axial loading.

Fig. 2 Geometry and coordinates of the DWCNT under axial loading



Consider the fluid flow in a CNTRC cylindrical shell in which the flow is assumed to be axially symmetric, Newtonian and laminar [63]. By the well-known Navier–Stokes equation, the basic momentum governing equation of the flow is simplified as:

$$\rho_b \frac{dV_R}{dt} = -\frac{\partial P}{\partial R} + \frac{1}{R} \frac{\partial \tau_{R\theta}}{\partial \theta} - \frac{\tau_{\theta\theta}}{R} + \frac{\partial \tau_{Rx}}{\partial x} \tag{10}$$

In Eq. (10), P and ρ_b are pressure and mass density of the fluid, respectively. The fluid force acting on the SWCNT can be calculated from Eq. (10). Since the acceleration and the velocity of the SWCNT and fluid at the contact point are equal [63], there are below relations:

$$v_R = \frac{dw}{dt}, \quad \frac{d}{dt} = \frac{\partial}{\partial t} + v_x \frac{\partial}{\partial x} \tag{11}$$

where v_x is the mean flow velocity. In Eq. (11), shear stress (τ) depends on the viscosity (μ) which can be obtained as below:

$$\tau_{R\theta} = \mu \frac{\partial V_R}{\partial \theta}, \quad \tau_{\theta\theta} = 2\mu \frac{V_R}{R}, \quad \tau_{Rx} = \mu \frac{\partial V_R}{\partial x} \tag{12}$$

Finally, using Eqs. (11) and (12) and combining them with Eq. (10), the pressure of fluid ($\frac{\partial P}{\partial R}$) will be obtained. The fluid flow work can be written as:

$$\delta W_2 = \int_0^{2\pi} \int_0^L \frac{\partial P}{\partial R} R dx d\theta \tag{13}$$

The axial fluid velocity in the above relation can be written as:

$$v_x = v_{ave,slip} = VCF \times v_{ave,noslip} \tag{14}$$

where the modified dimensionless coefficient VCF may be defined as [64]:

$$VCF = (1 + aK_n) \times \left[1 + 4 \left(\left(\frac{2 - \sigma_v}{\sigma_v} \right) \left(\frac{k_n}{1 + k_n} \right) \right) \right] \tag{15}$$

where the slip of flow from inner SWCNT is considered through the Knudsen number (k_n). Practically, it is supposed to be $\sigma_v = 0.7$; in addition, other parameters are:

$$a = a_0 \frac{2}{\pi} (\tan^{-1}(a_1 k_n^b)), \quad a_0 = \frac{64}{3\pi} \left(1 - \frac{4}{b} \right)^{-1}, \quad \mu = \mu_0 (1 + a k_n)^{-1} \tag{16}$$

In Eq. (16), μ and μ_0 are fluid viscosity and bulk viscosity, respectively. The work done by Pasternak foundation, as the surrounding medium acting on the DWCNT, can be expressed as [41]:

$$\delta W_3 = \{K_w w + K_p \nabla^2 w\} \delta w R dV, \quad \nabla^2 = \frac{\partial^2}{\partial x^2} + \frac{1}{R^2} \frac{\partial^2}{\partial \theta^2} \tag{17}$$

in which K_w and K_p are the Winkler and Pasternak coefficients, respectively. The energy dissipated by the dampers acting on DWCNT by the surrounding medium can be expressed as [41]:

$$\delta D = \iiint_V \left\{ C_d \frac{\partial w}{\partial t} \frac{\partial}{\partial t} \delta w \right\} R dV \tag{18}$$

in which C_d is the damping constant. Now equations of motion and boundary conditions can be obtained by substituting Eqs. (6), (8), (9), (13), (17) and (18) into (4) and integrating by parts.

For inner nanotube:

$$\begin{aligned}
\delta u_1 &: \frac{\partial N_{xx}^1}{\partial x} + \frac{1}{R} \frac{\partial N_{x\theta}^1}{\partial \theta} + \frac{1}{2R^2} \left(-\frac{\partial Y_{\theta\theta}^1}{\partial \theta} + \frac{\partial Y_{zz}^1}{\partial \theta} \right) + \frac{1}{2R} \frac{\partial^2 Y_{zx}^1}{\partial \theta \partial x} + \frac{1}{2R^2} \frac{\partial^2 Y_{\theta z}^1}{\partial \theta^2} \\
&= I_0^1 \frac{\partial^2 u_1}{\partial t^2} + I_1^1 \frac{\partial^2 \psi_{1x}}{\partial t^2} \\
\delta v_1 &: \frac{\partial N_{x\theta}^1}{\partial x} + \frac{1}{R} \frac{\partial}{\partial \theta} N_{\theta\theta}^1 + \frac{Q_{z\theta}^1}{R} + \frac{1}{2} \left\{ \frac{1}{R} \frac{\partial}{\partial x} (-Y_{xx}^1 + Y_{\theta\theta}^1) \right. \\
&\quad \left. - \frac{1}{R^2} \frac{\partial Y_{\theta x}^1}{\partial \theta} - \frac{\partial^2 Y_{xz}^1}{\partial x^2} - \frac{Y_{xz}^1}{R^2} - \frac{1}{R} \frac{\partial^2 Y_{z\theta}^1}{\partial \theta \partial x} \right\} \\
&= I_0^1 \left[\frac{\partial^2 v_1}{\partial t^2} \right] + I_1^1 \left\{ \frac{\partial^2 \psi_{1\theta}}{\partial t^2} \right\} \\
\delta w_1 &: \frac{\partial Q_{xz}^1}{\partial x} + \frac{1}{R} \frac{\partial Q_{z\theta}^1}{\partial \theta} - \frac{N_{\theta\theta}^1}{R} - \frac{1}{2R^2} \frac{\partial^2 Y_{\theta x}^1}{\partial \theta^2} - \frac{1}{2R^2} \frac{\partial Y_{zx}^1}{\partial \theta} + \frac{1}{2R} \frac{\partial Y_{\theta z}^1}{\partial x} + \frac{\partial^2 Y_{x\theta}^1}{2\partial x^2} \\
&\quad - \frac{1}{2R} \frac{\partial^2}{\partial \theta \partial x} (Y_{xx}^1 - Y_{\theta\theta}^1) - \zeta_1 v_x^2 \frac{\partial^2 w_1}{\partial x^2} - \zeta_2 v_x \frac{\partial w_1}{\partial x} + \zeta_3 v_x \frac{\partial^3 w_1}{\partial x^3} - K_1 (w_1 - w_2) + \bar{F} \left(\frac{\partial^2 w}{\partial x^2} + \frac{\partial^2 v}{\partial x^2} \right) \\
&\quad + K_{1p} \nabla^2 (w_1 - w_2) - C_{1d} \left(\frac{\partial w_1}{\partial t} - \frac{\partial w_2}{\partial t} \right) = I_0^1 \left(\frac{\partial^2 w_1}{\partial t^2} \right) + \zeta_4 \frac{\partial^2 w_1}{\partial t^2} - \zeta_5 v_x \frac{\partial^2 w_1}{\partial x \partial t} - \zeta_6 \frac{\partial w_1}{\partial t} + \zeta_7 \frac{\partial^3 w_1}{\partial t \partial x^2} \\
\delta \psi_{1x} &: \frac{\partial M_{xx}^1}{\partial x} + \frac{1}{R} \frac{\partial M_{\theta\theta}^1}{\partial \theta} - Q_{xz}^1 + \frac{1}{2} \frac{\partial Y_{\theta x}^1}{\partial x} - \frac{1}{2R} \frac{\partial}{\partial \theta} (Y_{zz}^1 - Y_{\theta\theta}^1) + \frac{Y_{zz}^1}{R} + \frac{1}{2R} \frac{\partial^2 T_{zx}^1}{\partial \theta \partial x} + \frac{1}{2R^2} \frac{\partial^2 T_{\theta z}^1}{\partial \theta^2} \\
&= I_1^1 \frac{\partial^2 u_1}{\partial t^2} + I_2^1 \frac{\partial^2 \psi_{1x}}{\partial t^2} \\
\delta \psi_{1\theta} &: \frac{1}{R} \frac{\partial M_{\theta\theta}^1}{\partial \theta} + \frac{\partial M_{x\theta}^1}{\partial x} - Q_{z\theta}^1 + \frac{1}{2} \frac{\partial}{\partial x} \left(Y_{zz}^1 - Y_{xx}^1 + \frac{T_{\theta\theta}^1}{R} \right) - \frac{1}{2} \frac{\partial Y_{\theta x}^1}{\partial \theta} + \frac{Y_{xz}^1}{2R} - \frac{1}{2R} \frac{\partial^2 T_{\theta z}^1}{\partial \theta \partial x} - \frac{1}{2} \frac{\partial^2 T_{zx}^1}{\partial x^2} \\
&= I_1^1 \left(\frac{\partial^2 v_1}{\partial t^2} \right) + I_2^1 \left(\frac{\partial^2 \psi_{1\theta}}{\partial t^2} \right)
\end{aligned} \tag{19}$$

For outer nanotube:

$$\begin{aligned}
\delta u_2 &: \frac{\partial N_{xx}^2}{\partial x} + \frac{1}{R} \frac{\partial N_{x\theta}^2}{\partial \theta} + \frac{1}{2R^2} \left(-\frac{\partial Y_{\theta\theta}^2}{\partial \theta} + \frac{\partial Y_{zz}^2}{\partial \theta} \right) + \frac{1}{2R} \frac{\partial^2 Y_{zx}^2}{\partial \theta \partial x} + \frac{1}{2R^2} \frac{\partial^2 Y_{\theta z}^2}{\partial \theta^2} \\
&= I_0^2 \frac{\partial^2 u_2}{\partial t^2} + I_1^2 \frac{\partial^2 \psi_{2x}}{\partial t^2} \\
\delta v_2 &: \frac{\partial N_{x\theta}^2}{\partial x} + \frac{1}{R} \frac{\partial}{\partial \theta} N_{\theta\theta}^2 + \frac{Q_{z\theta}^2}{R} + \frac{1}{2} \left\{ \frac{1}{R} \frac{\partial}{\partial x} (-Y_{xx}^2 + Y_{\theta\theta}^2) \right. \\
&\quad \left. - \frac{1}{R^2} \frac{\partial Y_{\theta x}^2}{\partial \theta} - \frac{\partial^2 Y_{xz}^2}{\partial x^2} - \frac{Y_{xz}^2}{R^2} - \frac{1}{R} \frac{\partial^2 Y_{z\theta}^2}{\partial \theta \partial x} \right\} \\
&= I_0^2 \left[\frac{\partial^2 v_2}{\partial t^2} \right] + I_1^2 \left\{ \frac{\partial^2 \psi_{2\theta}}{\partial t^2} \right\} \\
\delta w_2 &: \frac{\partial Q_{xz}^2}{\partial x} + \frac{1}{R} \frac{\partial Q_{z\theta}^2}{\partial \theta} - \frac{N_{\theta\theta}^2}{R} - \frac{1}{2R^2} \frac{\partial^2 Y_{\theta x}^2}{\partial \theta^2} - \frac{1}{2R^2} \frac{\partial Y_{zx}^2}{\partial \theta} + \frac{1}{2R} \frac{\partial Y_{\theta z}^2}{\partial x} + \frac{\partial^2 Y_{x\theta}^2}{2\partial x^2} + \bar{F} \left(\frac{\partial^2 w}{\partial x^2} + \frac{\partial^2 v}{\partial x^2} \right) \\
&\quad - \frac{1}{2R} \frac{\partial^2}{\partial \theta \partial x} (Y_{xx}^2 - Y_{\theta\theta}^2) - K_1 (w_2 - w_1) + K_{1p} \nabla^2 (w_2 - w_1) - C_{1d} \left(\frac{\partial w_2}{\partial t} - \frac{\partial w_1}{\partial t} \right) - K_2 (w_2) \\
&\quad + K_{2p} \nabla^2 (w_2) - C_{2d} \left(\frac{\partial w_2}{\partial t} \right) = I_0^2 \left(\frac{\partial^2 w_2}{\partial t^2} \right) \\
\delta \psi_{2x} &: \frac{\partial M_{xx}^2}{\partial x} + \frac{1}{R} \frac{\partial M_{\theta\theta}^2}{\partial \theta} - Q_{xz}^2 + \frac{1}{2} \frac{\partial Y_{\theta x}^2}{\partial x} - \frac{1}{2R} \frac{\partial}{\partial \theta} (Y_{zz}^2 - Y_{\theta\theta}^2) + \frac{Y_{zz}^2}{R} + \frac{1}{2R} \frac{\partial^2 T_{zx}^2}{\partial \theta \partial x} + \frac{1}{2R^2} \frac{\partial^2 T_{\theta z}^2}{\partial \theta^2} \\
&= I_1^2 \frac{\partial^2 u_2}{\partial t^2} + I_2^2 \frac{\partial^2 \psi_{2x}}{\partial t^2} \\
\delta \psi_{2\theta} &: \frac{1}{R} \frac{\partial M_{\theta\theta}^2}{\partial \theta} + \frac{\partial M_{x\theta}^2}{\partial x} - Q_{z\theta}^2 + \frac{1}{2} \frac{\partial}{\partial x} \left(Y_{zz}^2 - Y_{xx}^2 + \frac{T_{\theta\theta}^2}{R} \right) - \frac{1}{2} \frac{\partial Y_{\theta x}^2}{\partial \theta} + \frac{Y_{xz}^2}{2R} - \frac{1}{2R} \frac{\partial^2 T_{\theta z}^2}{\partial \theta \partial x} - \frac{1}{2} \frac{\partial^2 T_{zx}^2}{\partial x^2} \\
&= I_1^2 \left(\frac{\partial^2 v_2}{\partial t^2} \right) + I_2^2 \left(\frac{\partial^2 \psi_{2\theta}}{\partial t^2} \right)
\end{aligned} \tag{20}$$

Also, associated boundary conditions for each nanotube are as below:

$$\begin{aligned}
 \delta u = 0 \quad \text{or} \quad & \left(N_{xx} + \frac{1}{4R} \frac{\partial Y_{xz}}{\partial \theta} \right) n_x + \left(N_{x\theta} - \frac{Y_{\theta\theta} - Y_{zz}}{2R} + \frac{1}{4} \frac{\partial Y_{xz}}{\partial x} + \frac{1}{2R} \frac{\partial Y_{\theta z}}{\partial \theta} \right) n_\theta = 0, \\
 \delta v = 0 \quad \text{or} \quad & \left(N_{x\theta} + \frac{Y_{\theta\theta} - Y_{xx}}{2R} - \frac{1}{2} \frac{\partial Y_{xz}}{\partial x} - \frac{1}{4R} \frac{\partial Y_{\theta z}}{\partial \theta} \right) n_x + \left(N_{\theta\theta} - \frac{1}{4R} \frac{\partial Y_{\theta z}}{\partial x} - \frac{Y_{\theta x}}{2R} \right) n_\theta = 0, \\
 \delta w = 0 \quad \text{or} \quad & \left(Q_{xz} + \frac{Y_{z\theta}}{2R} + \frac{1}{2} \frac{\partial Y_{x\theta}}{\partial x} + \frac{1}{4R} \frac{\partial(Y_{\theta\theta} - Y_{xx})}{\partial \theta} \right) n_x + \left(Q_{\theta z} - \frac{Y_{zx}}{2R} - \frac{1}{2R} \frac{\partial Y_{x\theta}}{\partial \theta} + \frac{1}{4} \frac{\partial(Y_{\theta\theta} - Y_{xx})}{\partial x} \right) n_\theta = 0, \\
 \delta \psi_x = 0 \quad \text{or} \quad & \left(M_{xx} + \frac{1}{4R} \frac{\partial T_{xz}}{\partial \theta} + \frac{Y_{x\theta}}{2} \right) n_x + \left(M_{\theta x} + \frac{1}{4} \frac{\partial T_{xz}}{\partial x} + \frac{1}{2R} \frac{\partial T_{\theta z}}{\partial \theta} + \frac{(Y_{\theta\theta} - Y_{zz})}{2} \right) n_\theta = 0, \\
 \delta \psi_\theta = 0 \quad \text{or} \quad & \left(M_{x\theta} - \frac{(Y_{xx} - Y_{zz})}{2} - \frac{1}{4R} \frac{\partial T_{\theta z}}{\partial \theta} - \frac{1}{2} \frac{\partial T_{xz}}{\partial x} + \frac{T_{\theta\theta}}{2R} \right) n_x + \left(M_{\theta\theta} - \frac{Y_{x\theta}}{2} - \frac{1}{4} \frac{\partial T_{\theta z}}{\partial x} \right) n_\theta = 0,
 \end{aligned}
 \tag{21}$$

According to this method, the approximate r-th derivative of f(x) is obtained by discretizing rule in the form of the linear sum of the function values as follows [68]:

For example:

The clamped boundary conditions at $x=0, L$:

$$u = v = w = \psi_x = \psi_\theta = 0 \tag{22}$$

The simply supported boundary conditions at $x=0, L$:

$$\begin{aligned}
 v = w = \psi_\theta = 0, \\
 \left(N_{xx} + \frac{1}{4R} \frac{\partial Y_{xz}}{\partial \theta} \right) = 0, \quad \left(M_{xx} + \frac{1}{4R} \frac{\partial T_{xz}}{\partial \theta} + \frac{Y_{x\theta}}{2} \right) = 0.
 \end{aligned}
 \tag{23}$$

The free boundary conditions at $x=0, L$:

$$\begin{aligned}
 \left(N_{xx} + \frac{1}{4R} \frac{\partial Y_{xz}}{\partial \theta} \right) = 0, \quad \left(M_{xx} + \frac{1}{4R} \frac{\partial T_{xz}}{\partial \theta} + \frac{Y_{x\theta}}{2} \right) = 0, \\
 \left(N_{x\theta} + \frac{Y_{\theta\theta} - Y_{xx}}{2R} - \frac{1}{2} \frac{\partial Y_{xz}}{\partial x} - \frac{1}{4R} \frac{\partial Y_{\theta z}}{\partial \theta} \right) = 0, \quad \left(Q_{xz} + \frac{Y_{z\theta}}{2R} + \frac{1}{2} \frac{\partial Y_{x\theta}}{\partial x} + \frac{1}{4R} \frac{\partial(Y_{\theta\theta} - Y_{xx})}{\partial \theta} \right) = 0, \\
 \left(M_{x\theta} - \frac{(Y_{xx} - Y_{zz})}{2} - \frac{1}{4R} \frac{\partial T_{\theta z}}{\partial \theta} - \frac{1}{2} \frac{\partial T_{xz}}{\partial x} + \frac{T_{\theta\theta}}{2R} \right) = 0
 \end{aligned}
 \tag{24}$$

$$\frac{d^r f(x)}{dx^r} \Big|_{x=x_p} = \sum_{j=1}^n C_{ij}^{(r)} f(x_j)
 \tag{25}$$

where n represents the number of distributed points along the x -axis and “ C_{ij} ” is the weighting coefficient calculated as below for the first-order derivative.

$$\begin{aligned}
 C_{ij}^{(1)} &= \frac{M(x_i)}{(x_i - x_j)M(x_j)} \quad i, j = 1, 2, \dots, n \text{ and } i \neq j \\
 C_{ij}^{(1)} &= - \sum_{j=1, j \neq i}^n C_{ij}^{(1)} \quad i = j
 \end{aligned}
 \tag{26}$$

3 Solution method

Differential quadrature method (DQM) was presented by Bellman et al. [65, 66] in 1970s. In this method, the precision of results depends on the numbers of grid points. In the preliminary version, the weighting coefficients were established using an algebraic equation which limited the utilization of large numbers of grid points. Shu [67] introduced a new method using an explicit formula for the weighting coefficients with infinite number of grid points which is known as GDQ. Shu and Richards [68] employed a new domain decomposition technique that can be applied in multi-domain problems. In this article, GDQ method is used in order to solve the governing equations under different boundary conditions.

where

$$M(x_i) = \prod_{j=1, j \neq i}^n (x_i - x_j) \tag{27}$$

In addition, the weighting coefficients for higher-order derivatives are determined by the following relations:

$$\begin{aligned}
 C_{ij}^{(r)} &= r \left[C_{ij}^{(r-1)} C_{ij}^{(1)} - \frac{C_{ij}^{(r-1)}}{(x_i - x_j)} \right] \quad i, j = 1, 2, \dots, n, i \neq j \text{ and } 2 \leq r \leq n - 1 \\
 C_{ii}^{(r)} &= - \sum_{j=1, j \neq i}^n C_{ij}^{(r)} \quad i, j = 1, 2, \dots, n \text{ and } 1 \leq r \leq n - 1
 \end{aligned}
 \tag{28}$$

For the free vibration of cylindrical shell analysis based on the first shear deformation theory, displacement field

Table 1 The comparison of the first three dimensionless natural frequencies of simply supported one-layer homogeneous isotropic nanoshells with different thicknesses. ($L=11.6$ nm, $L/R=5, =K_w=0$)

h/R	n	GDQ (present study)		[69]	GDQ (present study)
		$l=0$		$l=h$	
0.02	1	0.1954	0.19536215	0.1955	0.19543206
	2	0.2532	0.25271274	0.2575	0.25731258
	3	0.2772	0.27580092	0.3067	0.30621690
0.05	1	0.1959	0.19542305	0.1963	0.19585782
	2	0.2623	0.25884786	0.2869	0.28543902
	3	0.3220	0.31407326	0.4586	0.45457555

Table 2 The comparison of the first dimensionless natural frequencies of single-walled carbon nanotube with different thicknesses ($L=11.6$ nm, $L/R=5, K_w=l=0$ and $n=1$)

h/R	[70]	GDQM (present study)	Analytical (present study)
0.02	0.1968	0.19543206	0.1954320689
0.05	0.2004	0.1958578181	0.1958578259

Table 3 The effect of number of grid points on evaluating convergence of the natural frequency(GHz) of DWCNT with respect to boundary conditions (BCs) where $L_d/R_i=10, L_d/R_o=12.5, h_i=R_i/10, h_o=R_o/10, l_i=R_i/3, l_o=R_o/3, K_w i.o=1e10, K_p i.o=10, C_d i.o=100$

BCs	Velocity (m/s)	Axial load (N)	$N=9$	$N=11$	$N=13$	$N=15$	$N=17$	$N=19$	$N=21$
S-S	100	1	4.027144	4.027143	4.027143	4.027143	4.027143	4.027143	4.027143
	200	1.25	4.009631	4.009622	4.009624	4.009627	4.009628	4.009628	4.009628
	300	1.5	3.989036	3.989013	3.989018	3.989025	3.989028	3.989028	3.989028
	400	1.75	3.965276	3.965234	3.965244	3.965257	3.965261	3.965261	3.965261
C-C	100	1	4.437737	4.440442	4.440818	4.440756	4.440756	4.440756	4.440736
	200	1.25	4.421726	4.424398	4.424763	4.424699	4.424679	4.424679	4.424679
	300	1.5	4.402467	4.405119	4.405474	4.405408	4.405389	4.405403	4.405403
	400	1.75	4.379872	4.382516	4.382864	4.382794	4.382775	4.382795	4.382795

Table 4 The variations of first three natural frequencies versus flow velocity and length-to-radius ratio of a conveying fluid DWCNT where $h_i=R_i/10, h_o=R_o/10, l_i=R_i/3, l_o=R_o/3, K_w i.o=1e10, K_p i.o=10, C_d i.o=100$ and $F=1.75(N)$

		Fundamental frequency			Second frequency			Third frequency		
		$v=0$	300	600	$v=0$	300	600	$v=0$	300	600
S-S	$L_{i,o}/R_{i,o}$									
	8	4.3354	4.3217	4.281	9.4160	9.3911	9.3165	19.029	19.005	18.933
	10	3.9889	3.9756	3.9359	9.3478	9.3217	9.2425	18.955	18.938	18.857
	12	3.8270	3.813	3.7716	9.3133	9.2865	9.2043	18.914	18.897	18.816
C-C	$L_{i,o}/R_{i,o}$									
	8	4.9487	4.9342	4.8911	9.5256	9.5002	9.4262	19.064	19.043	18.968
	10	4.4077	4.3937	4.3519	9.4024	9.3762	9.2973	18.972	18.948	18.875
	12	4.1059	4.0916	4.0490	9.3442	9.3172	9.2349	18.924	18.908	18.826
	14	3.9305	3.9154	3.8708	9.3125	9.2851	9.2006	18.896	18.872	18.798

can be defined as follows due to the geometrical periodicity along θ direction

$$\begin{Bmatrix} u(x, \theta, t) \\ v(x, \theta, t) \\ w(x, \theta, t) \\ \psi_x(x, \theta, t) \\ \psi_\theta(x, \theta, t) \end{Bmatrix} = \sum_{n=1}^{\infty} \begin{Bmatrix} \bar{U}(x) \cos(n\theta)e^{i\omega t} \\ \bar{V}(x) \sin(n\theta)e^{i\omega t} \\ \bar{W}(x) \cos(n\theta)e^{i\omega t} \\ \bar{\Psi}_x(x) \cos(n\theta)e^{i\omega t} \\ \bar{\Psi}_\theta(x) \sin(n\theta)e^{i\omega t} \end{Bmatrix} \quad (29)$$

Substituting Eqs. (29) into governing equations, the following equation is achieved:

$$([M]\{\omega^2\} + [C]\{\omega\} + [K]) \begin{pmatrix} \beta_b \\ \beta_d \end{pmatrix} = 0 \quad (30)$$

Then GDQ is applied to the equations of motion and the boundary conditions to obtain the mass matrix $[M]$, damping matrix $[C]$ and stiffness matrix $[K]$. d and b indexes donate domain and boundary, respectively, and β shows the mode shape. A proper way for solving Eq. (30) is to rewrite it as follows:

$$\{\dot{Z}\} = \{A\}\{Z\} \tag{31}$$

in which state vector Z and state matrix $[A]$ are defined as:

$$Z = \left\{ \begin{matrix} d_d \\ \dot{d}_d \end{matrix} \right\} \text{ and } [A] = \begin{bmatrix} [0] & [I] \\ -[M^{-1}K] & -[M^{-1}C] \end{bmatrix} \tag{32}$$

In Eq. (32), $[0]$ and $[I]$ are the zero and unit (identity) matrices, respectively. Eventually, the natural frequency and its mode shape are obtained.

4 Results and discussion

4.1 Validation

The obtained results of present study need to be validated by the reports of previous researches. Therefore, in this section the first three natural frequencies of simply supported one-layer homogeneous isotropic nanoshell are compared with

ref [69]. These results are presented in Table 1. The comparison suggests that for both classical ($l=0$) and modified couple stress ($l=h$) theories, achieved responses by generalized differential quadrature method (GDQM) are verified by those of [69]. As another validation in Table 2, the first dimensionless natural frequencies of the single-walled carbon nanotube with different thicknesses reported by [70] are compared with obtained responses of GDQM and Navier analytical method in the present research. As can be seen, numerical and analytical responses are in good accordance with ref [70].

4.2 Convergence

In all figures and tables, $K_{wi} \cdot o$, $K_{pi} \cdot o$ and $C_{di} \cdot o$ are Winkler, Pasternak and damping coefficients of the inner and outer surfaces of DWCNT, respectively. In addition, L_i , L_o , R_i , R_o , h_i and h_o are the inner and outer lengths, radiuses and thicknesses of cylindrical shell, respectively. Table 3 shows the natural frequency variations versus the number of grid

Table 5 The variations of first three natural frequencies versus the axial load and radius-to-thickness of a conveying fluid DWCNT where $L_i/R_i=10$, $L_o/R_o=12.5$, $l_i=R_i/3$, $l_o=R_o/3$, $K_{wi} \cdot o=1e10$, $K_{pi} \cdot o=10$, $C_{di} \cdot o=100$ and $v=100$ m/s

		Fundamental frequency			Second frequency			Third frequency		
		$F=0$	1	2	$F=0$	1	2	$F=0$	1	2
S-S	$R_{i,o}/h_{i,o}$									
	0.1	4.0266	3.9733	3.9188	9.2959	9.2848	9.2738	18.892	18.888	18.883
	0.12	3.0693	3.0187	2.9667	6.9491	6.9376	6.9265	14.192	14.187	14.182
	0.14	2.5317	2.4843	2.4356	5.4664	5.4544	5.4424	11.178	11.173	11.168
	0.16	2.1975	2.1537	2.1086	4.4621	4.4497	4.4372	9.1116	9.1065	9.1015
C-C	$R_{i,o}/h_{i,o}$									
	0.1	4.4377	4.3912	4.3437	9.3515	9.3406	9.3283	18.913	18.905	18.901
	0.12	3.4947	3.4531	3.4105	7.0216	7.0096	6.9974	14.215	14.210	14.205
	0.14	2.9427	2.9052	2.8670	5.5571	5.5447	5.5321	11.207	11.202	11.197
	0.16	2.5803	2.5464	2.5118	4.5712	4.5585	4.5457	9.1468	9.1417	9.1366

Fig. 3 The variations of natural frequency versus the axial load of a conveying fluid DWCNT where $K_{wi} \cdot o=1e10$, $K_{pi} \cdot o=10$, $C_{di} \cdot o=100$, $v=100$ and simply supported boundary conditions in different length scales

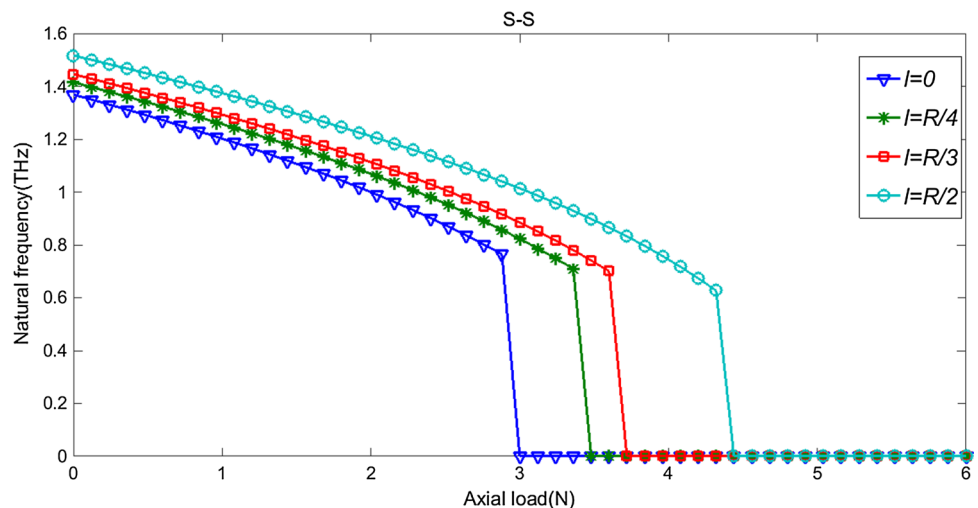


Fig. 4 The variations of natural frequency versus the axial load of a conveying fluid DWCNT where $K_w i \cdot o = 1e10$, $K_p i \cdot o = 10$, $C_d i \cdot o = 100$, $v = 100$ and clamped–clamped boundary conditions in different length scales

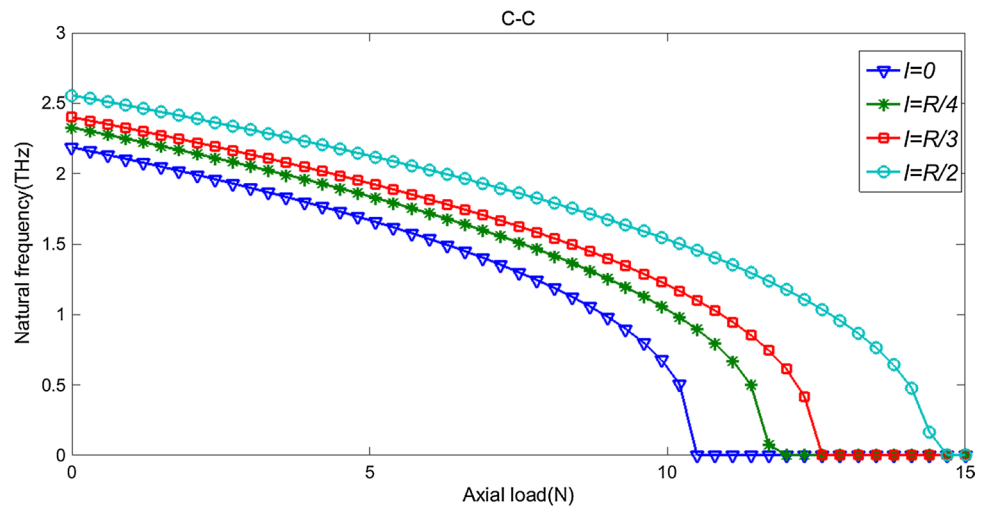


Fig. 5 The effect of material length scale on the critical flow velocity of a DWCNT where $K_w i \cdot o = 1e10$, $K_p i \cdot o = 10$, $C_d i \cdot o = 100$, $F = 1$ under different boundary conditions

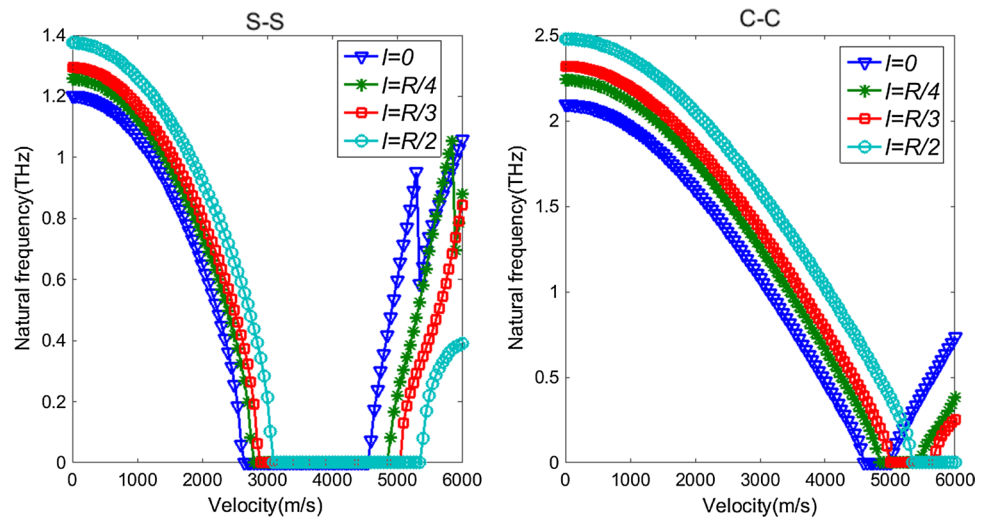
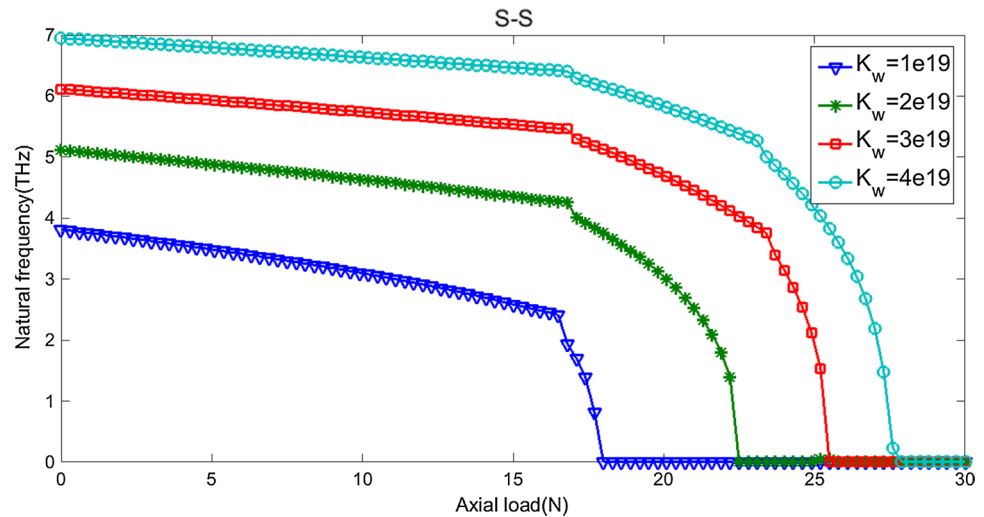


Fig. 6 The variations of natural frequency versus the axial load of a conveying fluid DWCNT where $K_p i \cdot o = 10$, $C_d i \cdot o = 100$, $v = 100$ m/s under simply supported boundary conditions, with the different constants of Winkler foundation



points for a double-walled carbon nanotube. This table indicates that $N = 19$ is enough for getting the convergent results; therefore, more grid points are not required. Table 1 also

shows that an increase in the fluid flow velocity and axial load reduces the natural frequency in clamped–clamped and simply supported boundary conditions.

Fig. 7 The variations of natural frequency versus the axial load of a conveying fluid DWCNT where $K_p i \cdot o = 10$, $C_d i \cdot o = 100$, $v = 100$, under clamped–clamped boundary conditions, with the different constants of Winkler foundation

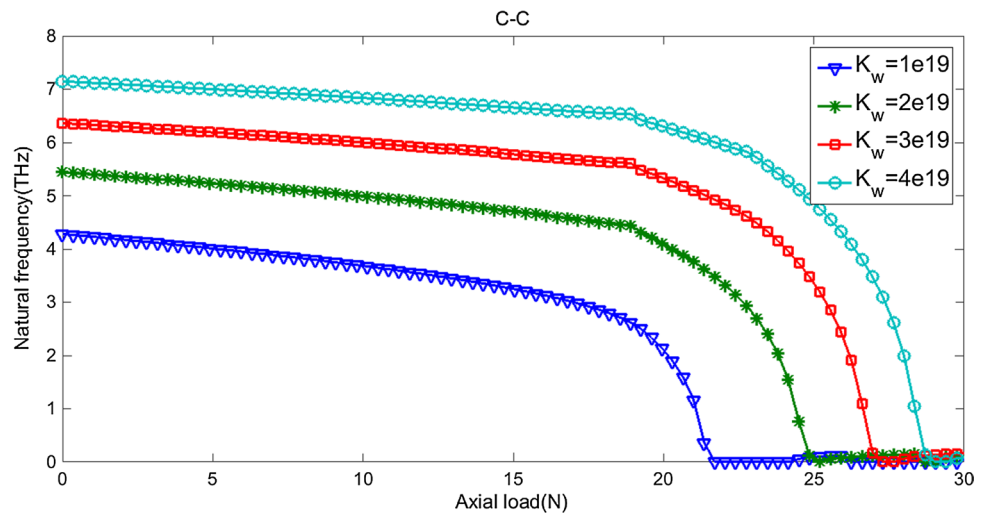
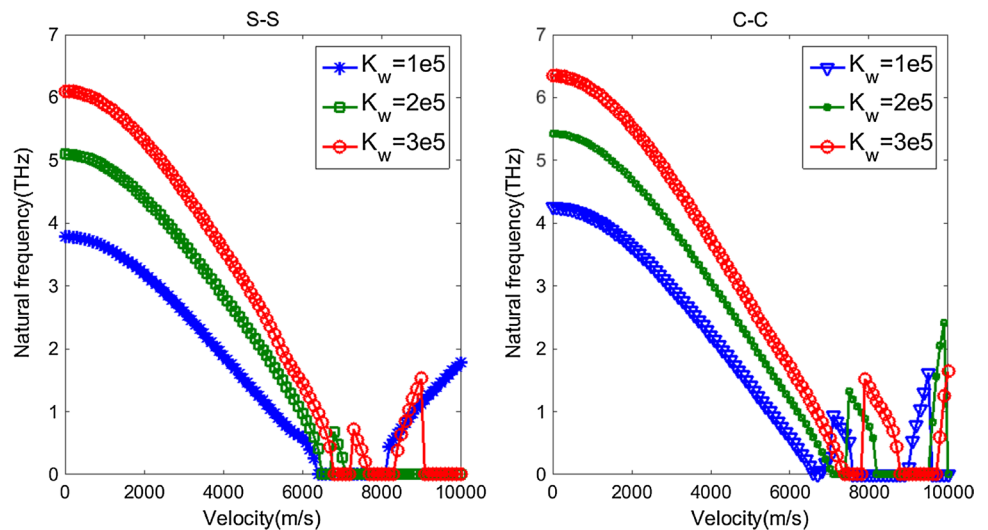


Fig. 8 The effect of Winkler foundation on the critical flow velocity of a DWCNT where $K_p i \cdot 10 = 10$, $C_d i \cdot o = 100$, $P = 0.5$, and under different boundary conditions



4.3 Parametric results

Table 4 provides some information on the effect of circumferential wave numbers, length-to-radius ratio and fluid flow velocity on natural frequency of a double-walled carbon nanotube conveying fluid under different boundary conditions. Increasing the modes of frequency leads to a considerable increase in natural frequency in both boundary conditions. This table also shows that an increase in the length-to-radius ratio is accompanied by decreasing the natural frequency due to a decrease in the rigidity of nanotube. Fluid flow velocity is the last parameter but not the least one which is investigated in Table 2, and results show its increase causes a decrease in the natural frequency in all modes, length-to-radius ratio and boundary conditions.

Table 5 shows the influences of circumferential wave numbers, radius-to-thickness and axial load on the natural frequency of a double-walled carbon nanotube conveying

fluid. As can be seen, the effect of the circumferential wave numbers is similar to the previous table and frequency increases significantly in the second and third modes. Another result achieved from Table 3 is that an increase in the radius-to-thickness leads to a decrease in natural frequency under the different axial loads and boundary conditions. In addition, increasing the axial load reduces the frequency especially in the first mode.

4.4 The effect of material length scale on the critical flow velocity and axial load

Figures 3 and 4 illustrate the effect of length-scale parameter on the natural frequency of a double-walled carbon nanotube conveying fluid. As can be seen, increasing the axial load natural frequency tends to decrease and eventually in a specific amount of load, known as the critical axial load, frequency drops to zero, and the buckling phenomenon

Fig. 9 The variations of natural frequency versus axial load of a conveying fluid DWCNT where $K_w i \cdot o = 1e10$, $C_d i \cdot o = 100$, $v = 100$, under simply supported boundary conditions, with the different constants of Pasternak foundation

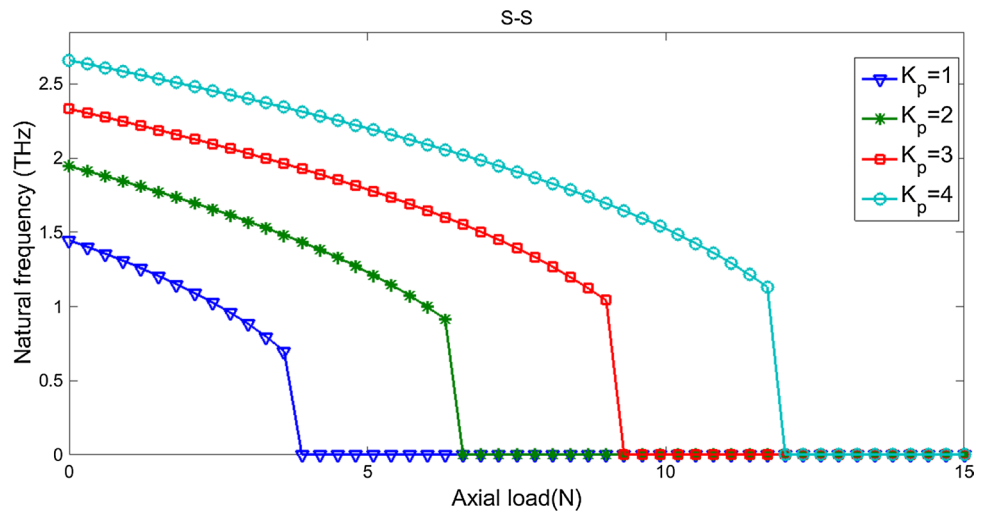


Fig. 10 The variations of natural frequency versus axial load of a conveying fluid DWCNT where $K_w i \cdot o = 1e10$, $C_d i \cdot o = 100$, $v = 100$ m/s, under clamped-clamped boundary conditions, with different constants of Pasternak foundation

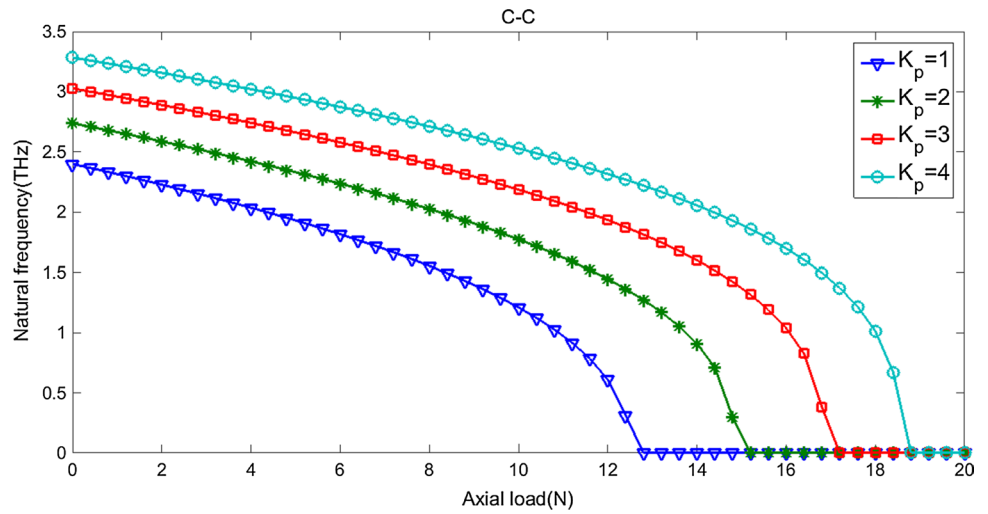


Fig. 11 The effect of Pasternak foundation on the critical flow velocity of a DWCNT where $K_w i \cdot o = 1e10$, $C_d i \cdot o = 100$, $F = 1$, under different boundary conditions

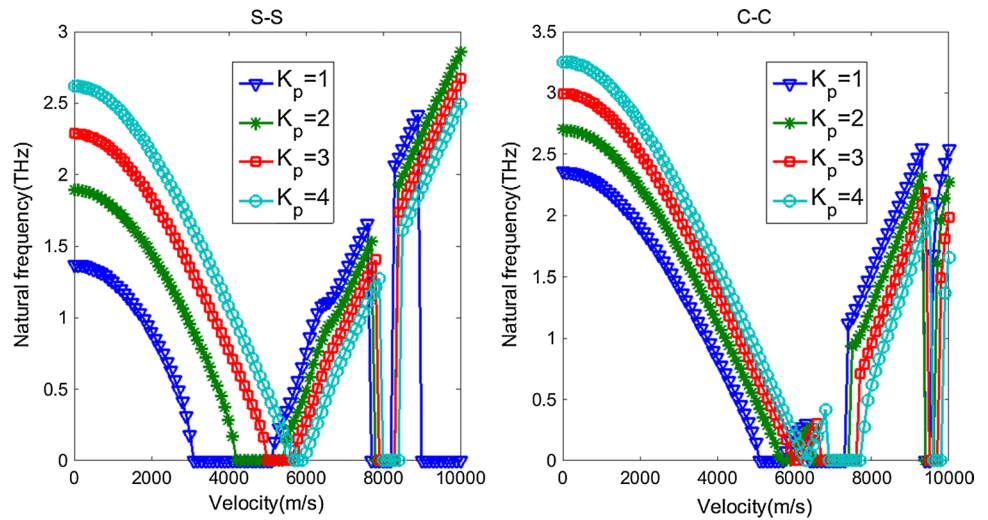


Fig. 12 The variations of natural frequency versus axial load of a conveying fluid DWCNT where $K_w i \cdot o = 1e10$, $K_p i \cdot o = 10$, $v = 100$, under simply supported boundary conditions, with the different constants of dampers

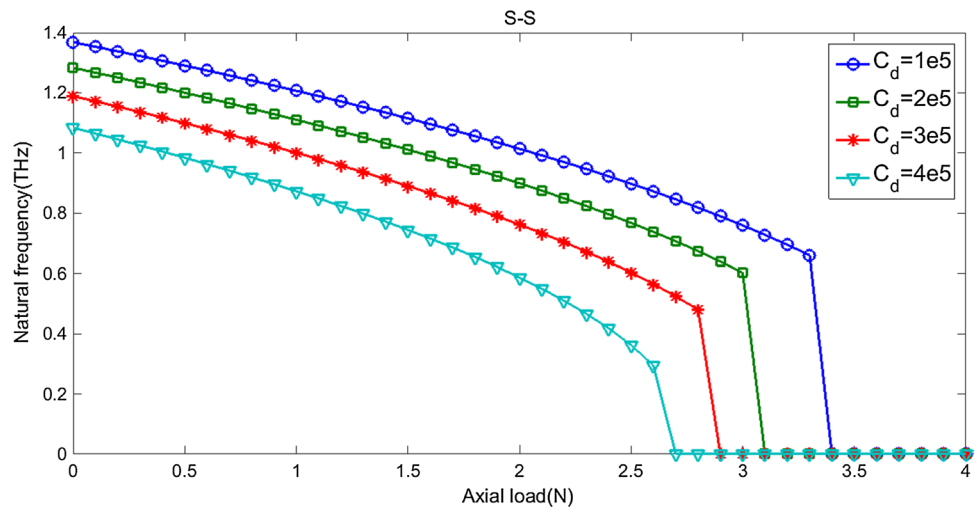


Fig. 13 The variations of natural frequency versus the axial load of a conveying fluid DWCNT where $K_w i \cdot o = 1e10$, $K_p i \cdot o = 10$, $v = 100$, under clamped-clamped boundary conditions, with the different constants of dampers

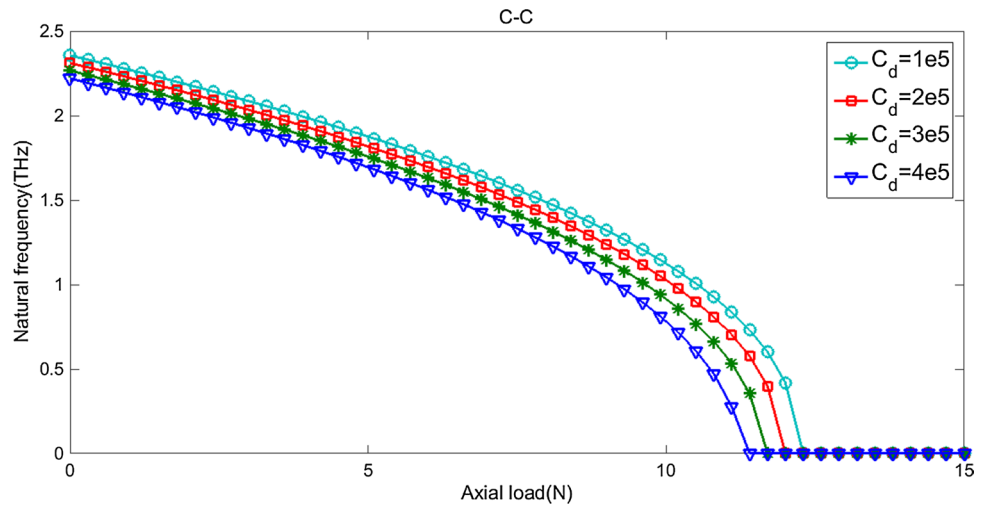
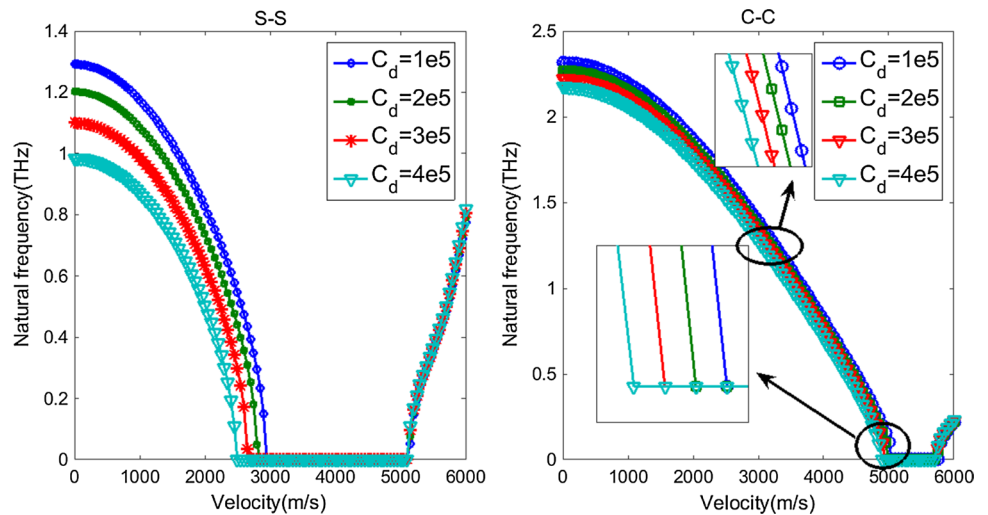


Fig. 14 The effect of dampers on the critical flow velocity of a DWCNT where $K_w i \cdot o = 1e10$, $K_p i \cdot o = 10$, $v = 0.5$, and under different boundary conditions



occurs. These figures also show that an increase in the material length scale enhances the natural frequency and critical buckling load. Figure 5 shows the effect of length-scale parameter on the natural frequency and critical flow velocity (the velocity in which frequency becomes zero) of a double-walled carbon. This figure expresses that an increase in the length-scale parameter also enhances the critical flow velocity and stability region.

4.5 The effect of Winkler foundation on the critical flow velocity and axial load

Figures 6, 7 and 8 illustrate the effect of Winkler foundation on the critical flow velocity and critical axial load of a double-walled carbon nanotube conveying fluid. These figures show that an increase in the Winkler foundation constant is coupled with an increase in the critical axial load and critical flow velocity. Figures 6 and 7 show that the influence of Winkler foundation on the critical axial load increase is stronger, when the constants of foundation are smaller. Another notable point is related to boundary conditions, natural frequencies, critical flow velocities and critical axial loads which are greater under the clamped–clamped boundary conditions because its rigidity is greater than simply supported.

4.6 The effect of Pasternak foundation on the critical flow velocity and axial load

Figures 9, 10 and 11 demonstrate the influence of Pasternak foundation on the critical flow velocity and critical axial load of a double-walled carbon nanotube conveying fluid. As can be seen in Figs. 9 and 10, an increase in the constant of Pasternak foundation increases the natural frequency and critical axial load. In simply supported boundary conditions, this increase is significantly stronger than clamped–clamped. Figure 11 shows that a similar trend occurs about the critical flow velocity, but the effect of foundation constants is more obvious in smaller constants, while the different foundation constants have almost equal effects on the critical axial load.

4.7 The effect of dampers on the critical flow velocity and axial load

Figures 12, 13 and 14 demonstrate the effect of dampers on the critical flow velocity and critical axial load of a double-walled carbon nanotube conveying fluid. It can be concluded from Figs. 12 and 13 that an increase in the dampers constant reduces the natural frequencies and critical axial loads, but decreasing the critical axial loads is more intense in the greater constants of dampers. Figure 14 shows that increasing the dampers constant leads the stability region to shrink

and the natural frequency to decrease. These effects are more obvious in simply supported boundary conditions.

5 Conclusion

This paper investigates the influences of fluid flow velocity and distributed axial load on the dynamic stability and buckling analysis of a viscoelastic double-walled carbon nanotube conveying viscous fluid. These effects are considered in one cylindrical shell model simultaneously for the first time. The nanotube is modeled as two orthotropic moderately thick cylindrical shells. The effects of small size and structural damping are considered based on the modified couple stress and Kelvin–Voigt theories. The elastic medium between the inner and outer layers of double-walled nanotube is simulated using visco-Pasternak foundation. The viscous fluid and its related forces are applied to formulation by modified Navier–Stokes relation, considering the slip boundary condition and Knudsen number. Finally, according to Hamilton's principle, the governing equations of motion and boundary conditions are derived and solved via both Navier and GDQM methods. The results show that the velocity of the viscous fluid flow, axial load, mode number, length-to-radius ratio, radius-to-thickness ratio, visco-Pasternak foundation and boundary conditions play an important role on the critical pressure and natural frequency of the viscoelastic DWCNT conveying viscous fluid flow and subjected to axial force.

References

1. Wang L, Ni Q, Li M (2008) Buckling instability of double-wall carbon nanotubes conveying fluid. *Comput Mater Sci* 44(2):821–825
2. Khosravian N, Rafii-Tabar H (2008) Computational modelling of a non-viscous fluid flow in a multi-walled carbon nanotube modelled as a Timoshenko beam. *Nanotechnology* 19(27):275703
3. Tang Y, Yang T (2018) Post-buckling behavior and nonlinear vibration analysis of a fluid-conveying pipe composed of functionally graded material. *Compos Struct* 185:393–400
4. Bauer S et al (2011) Size-effects in TiO₂ nanotubes: diameter dependent anatase/rutile stabilization. *Electrochem Commun* 13(6):538–541
5. Zienert A et al (2010) Transport in carbon nanotubes: contact models and size effects. *Physica Status Solidi B* 247(11–12):3002–3005
6. Xiao S, Hou W (2006) Studies of size effects on carbon nanotubes' mechanical properties by using different potential functions. *Fuller Nanotub Carbon Nonstruct* 14(1):9–16
7. Mohammadi K et al (2017) Comparison of modeling a conical nanotube resting on the Winkler elastic foundation based on the modified couple stress theory and molecular dynamics simulation. *Eur Phys J Plus* 132(3):115
8. Mohammadi K, Rajabpour A, Ghadiri M (2018) Calibration of nonlocal strain gradient shell model for vibration analysis of a

- CNT conveying viscous fluid using molecular dynamics simulation. *Comput Mater Sci* 148:104–115
9. Duan W, Wang C, Zhang Y (2007) Calibration of nonlocal scaling effect parameter for free vibration of carbon nanotubes by molecular dynamics. *J Appl Phys* 101(2):024305
 10. Vafamehr, A., et al., A framework for expansion planning of data centers in electricity and data networks under uncertainty. *IEEE Transactions on Smart Grid*, 2017
 11. Vafamehr A, Khodayar ME, Abdelghany K (2017) Oligopolistic competition among cloud providers in electricity and data networks. *IEEE Trans Smart Grid*. <https://doi.org/10.1109/TSG.2017.2778027>
 12. Vafamehr A, Khodayar ME (2018) Energy-aware cloud computing. *Electr J* 31(2):40–49
 13. Eringen AC (1983) On differential equations of nonlocal elasticity and solutions of screw dislocation and surface waves. *J Appl Phys* 54(9):4703–4710
 14. Niknam H, Aghdam M (2015) A semi analytical approach for large amplitude free vibration and buckling of nonlocal FG beams resting on elastic foundation. *Compos Struct* 119:452–462
 15. Ghadiri M, Shafiei N (2017) Vibration analysis of a nano-turbine blade based on Eringen nonlocal elasticity applying the differential quadrature method. *J Vib Control* 23(19):3247–3265
 16. Salehipour H, Shahidi A, Nahvi H (2015) Modified nonlocal elasticity theory for functionally graded materials. *Int J Eng Sci* 90:44–57
 17. Ghadiri M, Shafiei N (2016) Nonlinear bending vibration of a rotating nanobeam based on nonlocal Eringen's theory using differential quadrature method. *Microsyst Technol* 22(12):2853–2867
 18. Shafiei N et al (2017) Vibration analysis of nano-rotor's blade applying Eringen nonlocal elasticity and generalized differential quadrature method. *Appl Math Model* 43:191–206
 19. Lee H-L, Chang W-J (2008) Free transverse vibration of the fluid-conveying single-walled carbon nanotube using nonlocal elastic theory. *J Appl Phys* 103(2):024302
 20. Arani AG et al (2013) Nonlinear nonlocal vibration of embedded DWCNT conveying fluid using shell model. *Physica B* 410:188–196
 21. Arani AG, Kolahchi R, Maraghi ZK (2013) Nonlinear vibration and instability of embedded double-walled boron nitride nanotubes based on nonlocal cylindrical shell theory. *Appl Math Model* 37(14–15):7685–7707
 22. Bahaadini R, Hosseini M (2016) Effects of nonlocal elasticity and slip condition on vibration and stability analysis of viscoelastic cantilever carbon nanotubes conveying fluid. *Comput Mater Sci* 114:151–159
 23. Tang Y, Yang T (2018) Bi-directional functionally graded nanotubes: fluid conveying dynamics. *Int J Appl Math* 10(4):1850041
 24. Wang L et al (2016) Natural frequency and stability tuning of cantilevered CNTs conveying fluid in magnetic field. *Acta Mech Solida Sin* 29(6):567–576
 25. Askari H, Esmailzadeh E (2017) Forced vibration of fluid conveying carbon nanotubes considering thermal effect and nonlinear foundations. *Compos B Eng* 113:31–43
 26. Zang J et al (2014) Longitudinal wave propagation in a piezoelectric nanoplate considering surface effects and nonlocal elasticity theory. *Physica E* 63:147–150
 27. Zhang Y-W et al (2017) Quantum effects on thermal vibration of single-walled carbon nanotubes conveying fluid. *Acta Mech Solida Sin* 30(5):550–556
 28. Azrar A, Azrar L, Aljinaidi AA (2015) Numerical modeling of dynamic and parametric instabilities of single-walled carbon nanotubes conveying pulsating and viscous fluid. *Compos Struct* 125:127–143
 29. Mirafzal A, Fereidoon A, Andalib E (2018) Nonlocal dynamic stability of DWCNTs containing pulsating viscous fluid including surface stress and thermal effects based on sinusoidal higher order shear deformation shell theory. *J Mech* 34(3):387–398
 30. Miandoab EM et al (2014) Polysilicon nano-beam model based on modified couple stress and Eringen's nonlocal elasticity theories. *Physica E* 63:223–228
 31. Zeighampour H, Beni YT (2014) Cylindrical thin-shell model based on modified strain gradient theory. *Int J Eng Sci* 78:27–47
 32. Gholami R et al (2014) Size-dependent axial buckling analysis of functionally graded circular cylindrical microshells based on the modified strain gradient elasticity theory. *Meccanica* 49(7):1679–1695
 33. Zeighampour H, Beni YT, Karimpour I (2016) Torsional vibration and static analysis of the cylindrical shell based on strain gradient theory. *Arab J Sci Eng* 41(5):1713–1722
 34. Gholami R et al (2016) Vibration and buckling of first-order shear deformable circular cylindrical micro-/nano-shells based on Mindlin's strain gradient elasticity theory. *Eur J Mech-A/Solids* 58:76–88
 35. Zhang B et al (2015) Free vibration analysis of four-unknown shear deformable functionally graded cylindrical microshells based on the strain gradient elasticity theory. *Compos Struct* 119:578–597
 36. Barooti MM, Safarpour H, Ghadiri M (2017) Critical speed and free vibration analysis of spinning 3D single-walled carbon nanotubes resting on elastic foundations. *Eur Phys J Plus* 132(1):6
 37. Ghadiri M, Safarpour H (2016) Free vibration analysis of embedded magneto-electro-thermo-elastic cylindrical nanoshell based on the modified couple stress theory. *Appl Phys A* 122(9):833
 38. Ghadiri M, SafarPour H (2017) Free vibration analysis of size-dependent functionally graded porous cylindrical microshells in thermal environment. *J Therm Stresses* 40(1):55–71
 39. SafarPour H et al (2017) Influence of various temperature distributions on critical speed and vibrational characteristics of rotating cylindrical microshells with modified lengthscale parameter. *Eur Phys J Plus* 132(6):281
 40. Safarpour H et al (2018) Effect of porosity on flexural vibration of CNT-reinforced cylindrical shells in thermal environment using GDQM. *Int J Struct Stab Dyn* 18(10):1850123
 41. Zeighampour H, Beni YT (2014) Size-dependent vibration of fluid-conveying double-walled carbon nanotubes using couple stress shell theory. *Physica E* 61:28–39
 42. Ansari R et al (2015) Size-dependent vibration and instability of fluid-conveying functionally graded microshells based on the modified couple stress theory. *Microfluid Nanofluid* 19(3):509–522
 43. Tang M et al (2014) Nonlinear modeling and size-dependent vibration analysis of curved microtubes conveying fluid based on modified couple stress theory. *Int J Eng Sci* 84:1–10
 44. SafarPour H, Ghadiri M (2017) Critical rotational speed, critical velocity of fluid flow and free vibration analysis of a spinning SWCNT conveying viscous fluid. *Microfluid Nanofluid* 21(2):22
 45. Hu K et al (2016) Nonlinear and chaotic vibrations of cantilevered micropipes conveying fluid based on modified couple stress theory. *Int J Eng Sci* 105:93–107
 46. Guo Y, Xie J, Wang L (2018) Three-dimensional vibration of cantilevered fluid-conveying micropipes—types of periodic motions and small-scale effect. *Int J Non-Linear Mech* 102:112–135
 47. Yang T-Z et al (2014) Microfluid-induced nonlinear free vibration of microtubes. *Int J Eng Sci* 76:47–55
 48. Setoodeh A, Afrahim S (2014) Nonlinear dynamic analysis of FG micro-pipes conveying fluid based on strain gradient theory. *Compos Struct* 116:128–135
 49. Ghorbanpour Arani A et al (2016) Pulsating fluid induced dynamic instability of visco-double-walled carbon nano-tubes based on sinusoidal strain gradient theory using DQM and Bolotin method. *Int J Mech Mater Des* 12(1):17–38

50. Ansari R, Gholami R, Norouzzadeh A (2016) Size-dependent thermo-mechanical vibration and instability of conveying fluid functionally graded nanoshells based on Mindlin's strain gradient theory. *Thin-Walled Struct* 105:172–184
51. Ansari R et al (2016) Geometrically nonlinear free vibration and instability of fluid-conveying nanoscale pipes including surface stress effects. *Microfluid Nanofluid* 20(1):28
52. Ghazavi MR, Molki H, Ali beigloo A (2018) Nonlinear analysis of the micro/nanotube conveying fluid based on second strain gradient theory. *Appl Math Modell* 60:77–93
53. Li L et al (2016) Size-dependent effects on critical flow velocity of fluid-conveying microtubes via nonlocal strain gradient theory. *Microfluid Nanofluid* 20(5):76
54. Mohammadi K et al (2018) Cylindrical functionally graded shell model based on the first order shear deformation nonlocal strain gradient elasticity theory. *Microsyst Technol* 24(2):1133–1146
55. Mahinzare M et al (2017) Size-dependent effects on critical flow velocity of a SWCNT conveying viscous fluid based on nonlocal strain gradient cylindrical shell model. *Microfluid Nanofluid* 21(7):123
56. Sadeghi M, Thomassie R, Sasangohar F (2017) Objective assessment of functional information requirements for patient portals. In: *Proceedings of the human factors and ergonomics society annual meeting*. SAGE Publications Sage CA, Los Angeles, CA
57. Khanade K et al. (2017) Deriving information requirements for a smart nursing system for intensive care units. In: *Proceedings of the human factors and ergonomics society annual meeting*. SAGE Publications Sage CA, Los Angeles, CA
58. Sheng G, Wang X (2013) An analytical study of the non-linear vibrations of functionally graded cylindrical shells subjected to thermal and axial loads. *Compos Struct* 97:261–268
59. Jansen E, Rolfes R (2014) Non-linear free vibration analysis of laminated cylindrical shells under static axial loading including accurate satisfaction of boundary conditions. *Int J Non-Linear Mech* 66:66–74
60. Sofiyev A (2015) On the vibration and stability of shear deformable FGM truncated conical shells subjected to an axial load. *Compos B Eng* 80:53–62
61. Liang F, Su Y (2013) Stability analysis of a single-walled carbon nanotube conveying pulsating and viscous fluid with nonlocal effect. *Appl Math Model* 37(10–11):6821–6828
62. Torki ME et al (2014) Dynamic stability of functionally graded cantilever cylindrical shells under distributed axial follower forces. *J Sound Vib* 333(3):801–817
63. Rabani Bidgoli M, Saeed Karimi M, Ghorbanpour Arani A (2016) Nonlinear vibration and instability analysis of functionally graded CNT-reinforced cylindrical shells conveying viscous fluid resting on orthotropic Pasternak medium. *Mech Adv Mater Struct* 23(7):819–831
64. Fereidoon A, Andalib E, Mirafzal A (2016) Nonlinear vibration of viscoelastic embedded-DWCNTs integrated with piezoelectric layers-conveying viscous fluid considering surface effects. *Physica E* 81:205–218
65. Bellman R, Casti J (1971) Differential quadrature and long-term integration. *J Math Anal Appl* 34(2):235–238
66. Bellman R, Kashef B, Casti J (1972) Differential quadrature: a technique for the rapid solution of nonlinear partial differential equations. *J Comput Phys* 10(1):40–52
67. Shu C (2012) *Differential quadrature and its application in engineering*. Springer, Berlin
68. Shu C, Richards BE (1992) Application of generalized differential quadrature to solve two-dimensional incompressible Navier-Stokes equations. *Int J Numer Meth Fluids* 15(7):791–798
69. Tadi Beni Y, Mehralian F, Zeighampour H (2016) The modified couple stress functionally graded cylindrical thin shell formulation. *Mech Adv Mater Struct* 23(7):791–801
70. Alibeigloo A, Shaban M (2013) Free vibration analysis of carbon nanotubes by using three-dimensional theory of elasticity. *Acta Mech* 224(7):1415–1427

Publisher's Note Springer Nature remains neutral with regard to jurisdictional claims in published maps and institutional affiliations.